Downloaded from orbit.dtu.dk on: Apr 27, 2024

DTU Library

Estimating the parameters of globular cluster M 30 (NGC 7099) from time-series photometry

Kains, N.; Bramich, D.M.; Figuera Jaimes, R.; Arellano Ferro, A.; Figuera Jaimes, R.; Browne, P.; Dodds, P.; Dominik, M.; Hundertmark, M.; Liebig, C.

Total number of authors:
67

Published in:
Astronomy and Astrophysics

Link to article, DOI:
10.1051/0004-6361/201321819

Publication date:
2013

Document Version
Publisher's PDF, also known as Version of record

Link back to DTU Orbit

Citation (APA):
Kains, N., Bramich, D. M., Figuera Jaimes, R., Arellano Ferro, A., Figuera Jaimes, R., Browne, P., Dodds, P., Dominik, M., Hundertmark, M., Liebig, C., Jørgensen, U. G., Hardis, S., Harpsøe, K. B. W., Hinse, T. C., Juncher, D., Korhonen, H. H., Mathiasen, M. I. L., Skottfelt, J. M., Jørgensen, U. G., ... Vilela, C. (2013). Estimating the parameters of globular cluster M 30 (NGC 7099) from time-series photometry. *Astronomy and Astrophysics*, *555*, Article A36. https://doi.org/10.1051/0004-6361/201321819

General rights
Copyright and moral rights for the publications made accessible in the public portal are retained by the authors and/or other copyright owners and it is a condition of accessing publications that users recognise and abide by the legal requirements associated with these rights.

- Users may download and print one copy of any publication from the public portal for the purpose of private study or research.
- You may not further distribute the material or use it for any profit-making activity or commercial gain
- You may freely distribute the URL identifying the publication in the public portal

If you believe that this document breaches copyright please contact us providing details, and we will remove access to the work immediately and investigate your claim.

Astronomy & Astrophysics manuscript no. ngc7099
May 17, 2013
© ESO 2013

arXiv:1305.3606v1 [astro-ph.SR] 15 May 2013

Estimating the parameters of globular cluster M 30 (NGC 7099) from time-series photometry⋆,⋆⋆

N. Kains[1], D. M. Bramich[1], A. Arellano Ferro[2], R. Figuera Jaimes[1,3], U. G. Jørgensen[4,5], S. Giridhar[6] and
K.A. Alsubai[7], J. M. Andersen[8,5], V. Bozza[9,10], P. Browne[3], M. Burgdorf[11], S. Calchi Novati[9,12], Y. Damerdji[13], C. Diehl[14,15], P. Dodds[3], M. Dominik[3,⋆⋆⋆], A. Elyiv[13,16], X.-S. Fang[17,18], E. Giannini[14], S.-H. Gu[17,18], S. Hardis[4], K. Harpsøe[4,5], T.C. Hinse[19,4], A. Hornstrup[20], M. Hundertmark[3], J. Jessen-Hansen[21], D. Juncher[4,5], E. Kerins[22], H. Kjeldsen[21], H. Korhonen[4,5], C. Liebig[3], M. N. Lund[21], M. Lundkvist[21], L. Mancini[23], R. Martin[24], M. Mathiasen[4], M.T. Penny[25], M. Rabus[26], S. Rahvar[27,28], D. Ricci[29,13], K. Sahu[30], G. Scarpetta[9,31], J. Skottfelt[4,5], C. Snodgrass[32], J. Southworth[33], J. Surdej[13], J. Tregloan-Reed[33], C. Vilela[33], O. Wertz[13], and A. Williams[24]
(The MiNDSTEp consortium)

(Affiliations can be found after the references)

Received ... ; accepted ...

Abstract

Aims. We present the analysis of 26 nights of V and I time-series observations from 2011 and 2012 of the globular cluster M 30 (NGC 7099). We used our data to search for variable stars in this cluster and refine the periods of known variables; we then used our variable star light curves to derive values for the cluster's parameters.
Methods. We used difference image analysis to reduce our data to obtain high-precision light curves of variable stars. We then estimated the cluster parameters by performing a Fourier decomposition of the light curves of RR Lyrae stars for which a good period estimate was possible. We also derive an estimate for the age of the cluster by fitting theoretical isochrones to our colour-magnitude diagram (CMD).
Results. Out of 13 stars previously catalogued as variables, we find that only 4 are bona fide variables. We detect two new RR Lyrae variables, and confirm two additional RR Lyrae candidates from the literature. We also detect four other new variables, including an eclipsing blue straggler system, and an SX Phoenicis star. This amounts to a total number of confirmed variable stars in M 30 of 12. We perform Fourier decomposition of the light curves of the RR Lyrae stars to derive cluster parameters using empirical relations. We find a cluster metallicity $[\mathrm{Fe/H}]_{\mathrm{ZW}} = -2.01 \pm 0.04$, or $[\mathrm{Fe/H}]_{\mathrm{UVES}} = -2.11 \pm 0.06$, and a distance of 8.32 ± 0.20 kpc (using RR0 variables), 8.10 kpc (using one RR1 variable), and 8.35 ± 0.42 kpc (using our SX Phoenicis star detection in M 30). Fitting isochrones to the CMD, we estimate an age of 13.0 ± 1.0 Gyr for M 30.

Key words. globular clusters – RR Lyrae – variable stars

1. Introduction

In this paper we analyse time-series observations of M 30 (NGC 7099, or C2137-234 in the IAU nomenclature; $\alpha = 21^h40^m22^s, \delta = -23°10'47.5''$ at J2000.0), one of the most metal-poor globular clusters known, with [Fe/H] ∼ -2.1, located at a distance of ∼ 8 kpc. This cluster is thought to be of extra-Galactic origin, due to its retrograde orbit (Allen et al. 2006), pointing to its possible accretion by the Milky Way following an encounter with a satellite, as well as its position on the age-metallicity diagram (Forbes & Bridges 2010). M 30 is also thought to have undergone core collapse (e.g. Djorgovski & King 1986). Here we detect and classify already reported, as well as new variables, and use Fourier decomposition to derive properties of the RR Lyrae stars in this cluster. We then estimate the cluster parameters of M 30, providing us with an independent estimate of the metallicity, distance and age of this cluster, and the first using this method.

Our observations are detailed in Sec. 2; we discuss the variables in M 30 in Sec. 3, and in Sec. 4 we derive properties of the RR Lyrae stars in this cluster using Fourier decomposition and empirical relations. We use this to derive properties of the cluster in Sec. 5 and summarise our findings.

⋆ The full light curves presented in this paper (Table 2) are only available in electronic form at the Centre de données astronomiques de Strasbourg (CDS) via anonymous ftp to `cdsarc.u-strasbg.fr (130.79.128.5) or via http://cdsweb.u-strasbg.fr/cgi-bin/qcat?J/A+A/`

⋆⋆ This work is based on data collected by MiNDSTEp with the Danish 1.54m telescope at the ESO La Silla Observatory.

⋆⋆⋆ Royal Society University Research Fellow

Date	N_V	t_V(s)	N_I	t_I(s)
20110728	–	–	48	10
20110730	–	–	27	15-20
20110803	–	–	12	30
20110804	–	–	4	30
20110806	6	30	14	30
20110809	–	–	16	30-40
20110810	1	30	12	30
20110811	–	–	12	30
20110813	6	40	6	30
20110814	–	–	10	27
20110815	–	–	6	27
20110817	–	–	6	30
20110820	–	–	16	30
20110821	–	–	16	30
20110822	–	–	7	30
20110828	–	–	8	30
20110830	6	20	11	30
20110831	–	–	16	30
20120807	37	10-20	36	10-20
20120810	38	20	38	20
20120811	34	20	41	20
20120819	6	100	4	100
20120820	24	100	22	100
20120821	38	70-100	38	70-100
20120828	65	50-100	65	40-50
20120919	40	50	39	40
Total	301		530	

Table 1. Numbers of images and exposure times for the V and I band observations of M 30. When varying exposure times were used, a range is given.

2. Observations and reductions

2.1. Observations

We obtained Johnson V- and I-band data with the Danish Faint Object Spectrograph and Camera (DFOSC) imaging camera at the Danish 1.54m telescope at La Silla in Chile, as part of a programme with the MiNDSTEp consortium. In this programme we are making use of parts of the night when the MiNDSTEp primary-science microlensing observations towards the Galactic Bulge are not possible. The data were obtained in 2011 and 2012, with the 2011 data consisting mostly of I-band observations, while the 2012 observations are evenly split between V and I-band images. The observations are summarised in Table 1.

The imaging CCD is 2147 × 2101 pixel, with a scale of 0.396 arcsec per pixel, giving a field of view of 14.2 × 13.9 arcmin^2.

2.2. Difference image analysis

As in our previous studies of variables in globular clusters (Figuera et al. 2013, Kains et al. 2012; Arellano Ferro et al. 2011), we used the `DanDIA`[1] pipeline (Bramich et al. 2013; Bramich 2008) to reduce our observations. Using difference image analysis (DIA) enabled us to obtain high-precision photometry for sources within our field of view. The reader is referred to our previous papers (e.g. Bramich et al. 2011) for a detailed description of the software used; we provide a short summary of the main steps here.

[1] `DanDIA` is built from the `DanIDL` library of `IDL` routines available at `http://www.danidl.co.uk`

After preprocessing (bias level correction and flat-fielding), our images were blurred with a Gaussian of full-width half-maximum (FWHM) of 3 pixels to avoid undersampling, which is detrimental for determining the kernel in DIA. We then produce a reference image for each filter, stacking images within 10% of the best seeing ($\sim 1.2''$), also taking care to avoid including images with many saturated stars. Our reference image consists of 5 stacked images, with a combined exposure time of 100 s, and a FWHM of the point-spread function (PSF) of 3.88 pixels ($\sim 1.5''$) in V, while in I the combined exposure time is 80 s from 4 images, and the PSF FWHM is 3.31 pixels ($\sim 1.3''$). For each filter, the source positions and reference fluxes were then extracted from the reference image. Images were then registered with the reference, and the reference was convolved with the kernel solution and subtracted from each image, producing a set of difference images. Finally, difference fluxes were measured from each difference image for each source, which we used to construct a set of light curves. In Table 2, we outline the format of the data as it is provided in electronic format with the online version of this paper.

As was noted in previous papers, blending due to the presence of other objects near a source may lead to the reference flux being overestimated. However, non-variable sources are still fully subtracted in the difference images, while variable objects have the amplitude of their variability underestimated if their reference flux is affected by blending, although the shape of their light curve, crucially, will remain unaffected.

2.3. Photometric calibration

2.3.1. Self-calibration

Although all photometry is affected by systematic errors, steps can be taken to correct for this, in particular with time-series photometry, for which we can carry out a *self-calibration* of the data (e.g. Padmanabhan et al. 2008). To do this, we use the method of Bramich & Freudling (2012) to derive magnitude offsets to be applied to each photometric measurement. In practice, this equates to correcting for errors in the fitted value of the photometric scale factor p. We find magnitude offsets of the order of 2-3 mmag for most data points, which leads to small difference in the resulting light curves.

2.3.2. Photometric standards

We converted the instrumental magnitudes from our data reduction pipeline to standard Johnson-Kron-Cousins magnitudes by carrying out a linear fit to the relation between our light curve magnitudes and those of the photometric standards of Stetson (2000) in the field of this cluster. The relations, shown in Fig. 1, were used to obtain light curves in standard magnitudes. The standard stars we used cover the full range of colour and magnitude spanned by our CMD. No significant colour term was found and the correlation coefficients are ~ 1 for both filters.

2.4. Astrometry

We used GAIA to perform the astrometry by matching ∼400 manually picked stars from our reference images with

#	Filter	HJD (d)	$M_{\rm std}$ (mag)	$m_{\rm ins}$ (mag)	σ_m (mag)	$f_{\rm ref}$ (ADU s^{-1})	$\sigma_{\rm ref}$ (ADU s^{-1})	$f_{\rm diff}$ (ADU s^{-1})	$\sigma_{\rm diff}$ (ADU s^{-1})	p
V1	V	2455779.84508	15.360	14.475	0.004	4619.581	1.991	-500.380	4.612	0.3633
V1	V	2455779.84637	15.378	14.493	0.005	4619.581	1.991	-455.515	4.326	0.3185
⋮	⋮	⋮	⋮	⋮	⋮	⋮	⋮	⋮	⋮	⋮
V1	I	2455770.83621	14.628	14.797	0.007	2843.148	3.237	-68.927	2.472	0.1593
V1	I	2455770.83726	14.639	14.809	0.007	2843.148	3.237	-72.977	2.461	0.1593
⋮	⋮	⋮	⋮	⋮	⋮	⋮	⋮	⋮	⋮	⋮

Table 2. Format for the time-series photometry of all confirmed variables in our field of view. The standard $M_{\rm std}$ and instrumental $m_{\rm ins}$ magnitudes listed in columns 4 and 5 respectively correspond to the variable star, filter and epoch of mid-exposure listed in columns 1-3, respectively. The uncertainty on $m_{\rm ins}$ is listed in column 6, which also corresponds to the uncertainty on $M_{\rm std}$. For completeness, we also list the reference flux $f_{\rm ref}$ and the differential flux $f_{\rm diff}$ (columns 7 and 9 respectively), along with their uncertainties (columns 8 and 10), as well as the photometric scale factor p. Definitions of these quantities can be found in e.g. Bramich et al. (2011), Eq. 2-3. This is a representative extract from the full table, which is available with the electronic version of the article.

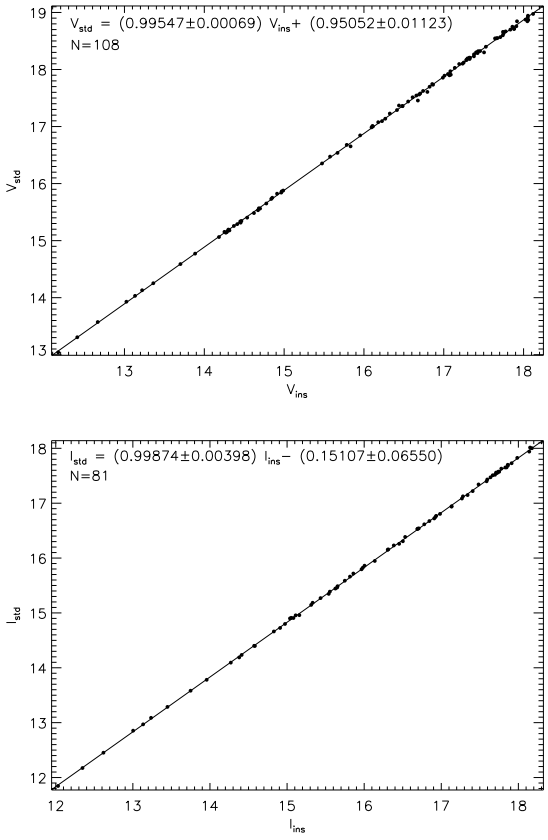

Figure 1. Linear regression fits used to convert from instrumental to standard Johnson-Kron-Cousins magnitudes for the V (top) and I (bottom) bands.

the USNO-B1.0 catalogue of stars (Monet et al. 2003) to derive a linear transformation between our image positions and equatorial coordinates. This means that the coordinates in Table 3 are given at the effective epoch of our reference image, HJD∼2456151.84. The root mean square (rms) of the residuals from our astrometric fit is 0.23 arcsec, or 0.59 pixels.

#	RA	DEC
V1	21:40:24.25	-23:11:46.4
V2	21:40:26.44	-23:12:51.2
V3	21:40:15.04	-23:11:27.9
V4	21:39:58.46	-23:11:43.3
V14	21:40:21.10	-23:11:30.8
V15	21:40:21.79	-23:10:50.1
V16	21:40:24.81	-23:11:48.8
V17	21:40:23.66	-23:11:01.1
V18	21:40:21.88	-23:09:32.4
V19	21:40:22.09	-23:10:43.3
V20	21:40:29.83	-23:11:05.9
V21	21:40:47.80	-23:10:23.9

Table 3. Equatorial celestial coordinates of confirmed variables in M 30 at the epoch of the reference image, HJD∼2456151.84.

3. Variables in M 30

The first three variables (V1-3) in this cluster were detected by Bailey (1902) using photographic observations made at the Harvard College Station in Arequipa, Peru. V4 was then reported by Rosino (1949), who discovered it using observations of M 30 at 175 epochs, taken between 1946 and 1948 with the 60cm reflecting telescope at the Lojano Astronomical Station, near Bologna in Italy. Rosino also derived periods for V1-3, and refined his period for V1 in a later paper (Rosino 1961). He also noted that V4 did not present the characteristics of an RR Lyrae type variable. He described it as an unusual object, reaching a magnitude of 16.4, remaining at that level for several days, before dropping below the limits of detectability of his photographic plates, i.e. below ∼ 18th magnitude. Other light curve features led him to conclude that V4 is a variable of type U Geminorum. This was confirmed in several subsequent publications by Margon & Downes (1983), who obtained spectroscopic evidence that V4 is a cataclysmic variable, and Machin et al. (1991), who also concluded that V4 is most likely a foreground object rather than a cluster member. Pietrukowicz et al. (2008) found a relatively high V-band brightness consistent with that assessment, and also noted that V4 has a likely X-ray counterpart detected by the *ROSAT* satellite.

Finally, V5-12 were all reported as variable by Terzan (1968), and V13 was reported by Terzan & Rutily (1975),

#	$< V >$	rms (V)	$< I >$	rms (I)
V5	17.42	0.035	16.75	0.047
V6	15.34	0.013	15.13	0.037
V7	16.63	0.021	15.84	0.018
V8	15.00	0.010	14.31	0.011
V9	15.40	0.012	15.08	0.021
V10	15.44	0.010	15.22	0.017
V11	16.11	0.013	15.25	0.012
V12	15.49	0.011	15.38	0.015
V13	15.69	0.040	14.78	0.030

Table 4. Mean magnitudes and rms limits for the stars previously catalogued as variable, but for which we do not find variability.

based on photographic observations taken at the 1.52m telescope at ESO between 1972 and 1974.; however they did not publish light curves or periods for any of those variables.

Pietrukowicz & Kaluzny (2004) analysed HST archival data of M 30 and identified two previously unknown RR Lyrae variables, as well as four W UMa-type contact binaries, and an eclipsing close-binary variable with ellipsoidal variations. However, they did not assign those variables catalogue V numbers. Finally, although Smitka & Layden (2010) also studied this cluster, their photometric accuracy is poor due to the cluster's low altitude for Northern hemisphere observations. They reported three new RR Lyrae star candidates, but did not provide coordinates or a finding chart, so we are not able to cross-correlate our findings with theirs; they also did not assign their variables V numbers.

This amounts to a total of 13 catalogued variables in the cluster, although V4 is now thought to be a foreground object. There are also 7 additional variables reported by Pietrukowicz & Kaluzny (2004), including 2 new RR Lyrae. The present study of M 30 is the first from the Southern hemisphere using CCD photometry, allowing us to carry out a significant update of the variable star population in this cluster.

3.1. Stars that do not show variability

We find that all of the stars V5-V13, reported by Terzan (1968) and Terzan & Rutily (1975) as variables, do not show signs of variability in our data, to within the limits of the rms scatter in our light curves; those limits are given in Table 4. We are also unable to detect variability of the five contact binaries listed by Pietrukowicz & Kaluzny (2004); for most of these, we attribute this to the fact that the variations have amplitudes of ~ 0.3 mag, for objects with $V \sim 20$ mag, which is very challenging to detect within the rms of our data (Fig. 2). This is especially difficult in the crowded central core, where blending leads to photon noise dominating any intrinsic variability signal. This is also true for the two brightest eclisping variables, which have V magnitudes of $\sim$17.3 and $\sim$17.9 and variation amplitudes of ~ 0.3 mag. The advent of electron-multiplying CCD (EMCCD) cameras, coupled with DIA, will allow us in the future to obtain high-quality photometry even for stars in the crowded cores of clusters Skottfelt et al. (2013), and to verify the variability status of these objects using ground-based photometry.

3.2. Detection of known variables

We recover the first three known RR Lyrae in this cluster (V1-V3) in our data, and calculate periods for each of them, using phase dispersion minimisation (PDM; Stellingwerf 1978) and the "string length" method (Lafler & Kinman 1965). In order to use the longest possible baseline to derive precise periods for these three variables, we used the data from Rosino (1949); these data are published in a table in that paper, and we provide them as an additional resource with the electronic version of this paper[2]. We also used these data to refine our periods by optimising the alignment in phase of that data set with ours; this is highly sensitive to the period, thanks to the baseline of $\sim$63 years. We also recovered the two additional RR Lyrae stars reported by Pietrukowicz & Kaluzny (2004) and assign them catalogue numbers V15 and V19, and calculated refined periods for these two stars. We note that V19 is highly blended due to its location in the very centre of the cluster, which explains its peculiar position on the CMD.

We also detect the U Gem variable V4, including some data taken during an outburst period. This star is discussed in more detail in Sec. 3.4.

3.3. Detection of new variables

As in our previous studies, we searched for new variables using three methods. Firstly, we constructed a stacked image S consisting of the sum of the absolute values of the deviations D of each image from the convolved reference image, divided by the pixel uncertainty σ, so that

$$S_{ij} = \sum_k \frac{|D_{kij}|}{\sigma_{kij}} \,. \quad (1)$$

Stars that deviate consistently from the reference image then stand out in this stacked image. Using this method, we discovered 2 new RR Lyrae stars, V14 and V16, both of RR1 type, with V16 also showing signs of amplitude and period modulation due to Blazhko effects or non-radial pulsation (see Sec. 3.4). Secondly, we inspected the light curves of objects which stand out on a plot of root mean square magnitude deviation versus mean magnitude, shown in Fig. 2.

Finally, we also searched for variables by conducting a period search for all our light curves using the string length method, and computing the ratio S_R of the string length for the best- to that of the worst-fit periods, with the smallest ratios expected for true periodic variations. We inspected visually all of the light curves of stars with $S_R < 0.55$, where the threshold value of 0.55 was chosen by inspecting the distribution of S_R (see Fig. 3). Using this method, we discovered V17, V18, V20 and V21.

All confirmed variables are listed in Table 5, in which we also give epochs, periods and amplitudes. The corresponding light curves are showin in Figs. 4 and 5. A finding chart of the cluster with the location of the confirmed variables is shown in Fig. 6, and a CMD showing the locations of all confirmed variables is shown in Fig. 7.

[2] The light curves for V1-V3 from Rosino (1949), as well as the additional data for V1 from Rosino (1961), are available in electronic form at the CDS via anonymous ftp to `cdsarc.u-strasbg.fr (130.79.128.5) or via http://cdsweb.u-strasbg.fr/cgi-bin/qcat?J/A+A/`

#	Epoch (HJD-2450000)	P (d)	P (Rosino 1949) (d)	P (Pietrukowicz et al. 2004) (d)	$< V >$ (mag)	$< I >$ (mag)	A_V (mag)	A_I (mag)	Type
V1	6160.8234	0.7436296	0.74365[a]	0.751	15.12	14.52	0.93	0.74	RR0
V2	6150.8616	0.6535119	0.6535049	–	15.20	14.62	0.92	0.65	RR0
V3	6147.8307	0.6963265	0.69632	–	15.12	14.54	0.94	0.67	RR0
V4[b]	6147.8569	0.092318	–	–	20.19	19.14	2.74	1.91	U Gem
V14	6150.8758	0.347953	–	–	15.18	14.77	0.48	0.32	RR1
V15	6160.7960	0.679015	–	0.689	15.07	14.52	1.08	0.68	RR0
V16	6190.7559	0.325366	–	–	15.22	14.81	0.33	0.27	RR1
V17	6150.8805	0.059954	–	–	14.14	13.08	0.07	0.04	SX Phoenicis + blend?
V18	6161.8536	0.307099	–	–	17.43	17.19	0.41	0.49	Eclipsing blue straggler
V19[c]	5779.8451	0.343379	–	0.341	13.85	13.10	0.15	0.11	RR1
V20	6147.8377	0.040199	–	–	17.79	17.57	0.15	0.13	SX Phoenicis
V21	6147.8589	0.113151	–	–	17.87	17.11	∼0.2	–	?

Table 5. Epochs, periods, mean magnitudes and amplitudes A in V and I for all confirmed variable stars in M 30. For RR Lyrae stars, $< V >$ and $< I >$ are intensity-weighted mean magnitudes, while for the other variables, they are inverse-variance-weighted mean magnitudes. [a]Rosino (1961) revised the period of V1 to 0.743608 d. [b]The period given for V4 is that of the sinusoidal variations seen during the quiescent part of the light curve, and the mean magnitudes are also those during quiescent phase; outburst mean magnitudes are given in the text (see Sec. 3.4). [c]For V19, the mean magnitudes are overestimated and amplitudes are underestimated due to blending, as discussed in the text.

3.4. Discussion of individual variables

We are unable to determine the nature of V17 with certainty. The combination of its position on the red giant branch and a short period of $\sim$ 0.06d makes it difficult to classify, although the shape of the light curve and the period would both be consistent with an SX Phoenicis variable blended with a red giant star (e.g. Darragh & Murphy 2012). This is difficult to quantify, and higher-resolution data would be needed to investigate that possibility. From the position of V18 on the CMD and its light curve showing minima of different depths, we suggest that it is an eclipsing blue straggler binary system, of which only 6 examples are known in globular clusters (Kai & Sheng-Bang 2012). We classify V20 as an SX Phoenicis variable, from its light curve, period, and position on the CMD; we only identify one pulsation period for this variable. We could not reach any conclusion as to the nature of V21, because of the quality of its light curve; however variability is clear from both the $V-$ and I-band light curves, when discarding the poor-quality 2011 data, and data with large error bars, from the I light curve. However we do verify that the variability of V21 is genuine in the difference images, and it is isolated, so there is no reason to believe that the variability is due to contamination from other variables. Below we discuss some of the variables in more detail.

3.4.1. V2

Figs. 4 and 5 show that our best period for V2 leads to an unsatisfactory phased light curve in both V and I. We suggest that the disjointed light curve may be due to a Blazhko effect (Blažko 1907) in this object; more observations are needed to confirm this.

3.4.2. V3

Like V2, but to a lesser extent, the light curves V3 seem disjointed, which we suggest may be due to a Blazhko effect. However, and more observations are needed to investigate this further.

3.4.3. V4

For the U Geminorum variable V4, we measured a quiet V-band median magnitude of 20.21 ± 0.48 mag, while during outburst, we find a median magnitude of 17.44 ± 0.04 mag, giving an amplitude of 2.74 mag; in the I band we find median values of 19.05 ± 0.40 (quiet) and 16.84 ± 0.48 (outburst), and an amplitude of 1.91 mag. Machin et al. (1991) found V4 to be significantly brighter, with $< V >_{\rm quiet} \sim$ 18.7 mag, and Pietrukowicz et al. (2008) also found $< V >_{\rm quiet} <$ 19 mag. It is interesting to note that, while our V data only covers one outburst, the I data covers three outburst, which show large variations in magnitude, by as much as $\sim$ 1 mag between different outbursts.

We also conducted a period search for the quiet part of the light curve; Machin et al. (1991) used the quiescent $B-V$ colour they find from their spectra of this object, and the relations of Echevarria & Jones (1984) between $B-V$ and P for dwarf novae, to conclude that the orbital period of V4 must be < 5 hours. We find a period during quiescence of $P = 0.0923$ days, or $P \sim 2.22$ hours, in agreement with that conclusion. In Fig. 8, we show the phased quiescent light curves with this period, while the unphased light curve is shown in Fig. 9.

3.4.4. V16

The light curves in both V and I suggest that our single best period does not lead to a satisfactory phased light curve; we discuss possible explanations for this here. First we considered the possibility that V16 might be a double-mode RR Lyrae (RR01) star, which have only been detected in a few Galactic globular clusters (e.g. Nemec 1985; Clement et al. 1993; Clementini et al. 2004, and references therein). To investigate this, a search for the fundamental and first-overtone pulsation periods was conducted using the string-length method. We start by conducting a period search to identify a first period; for this we find $P = 0.3254$. Assuming this to be the first-overtone period, and assuming an overtone-to-fundamental period ratio similar to what was found for double-mode RR Lyrae stars in M15, $P_1/P_0 \sim 0.748$ (Cox et al. 1983), we expect a funda-

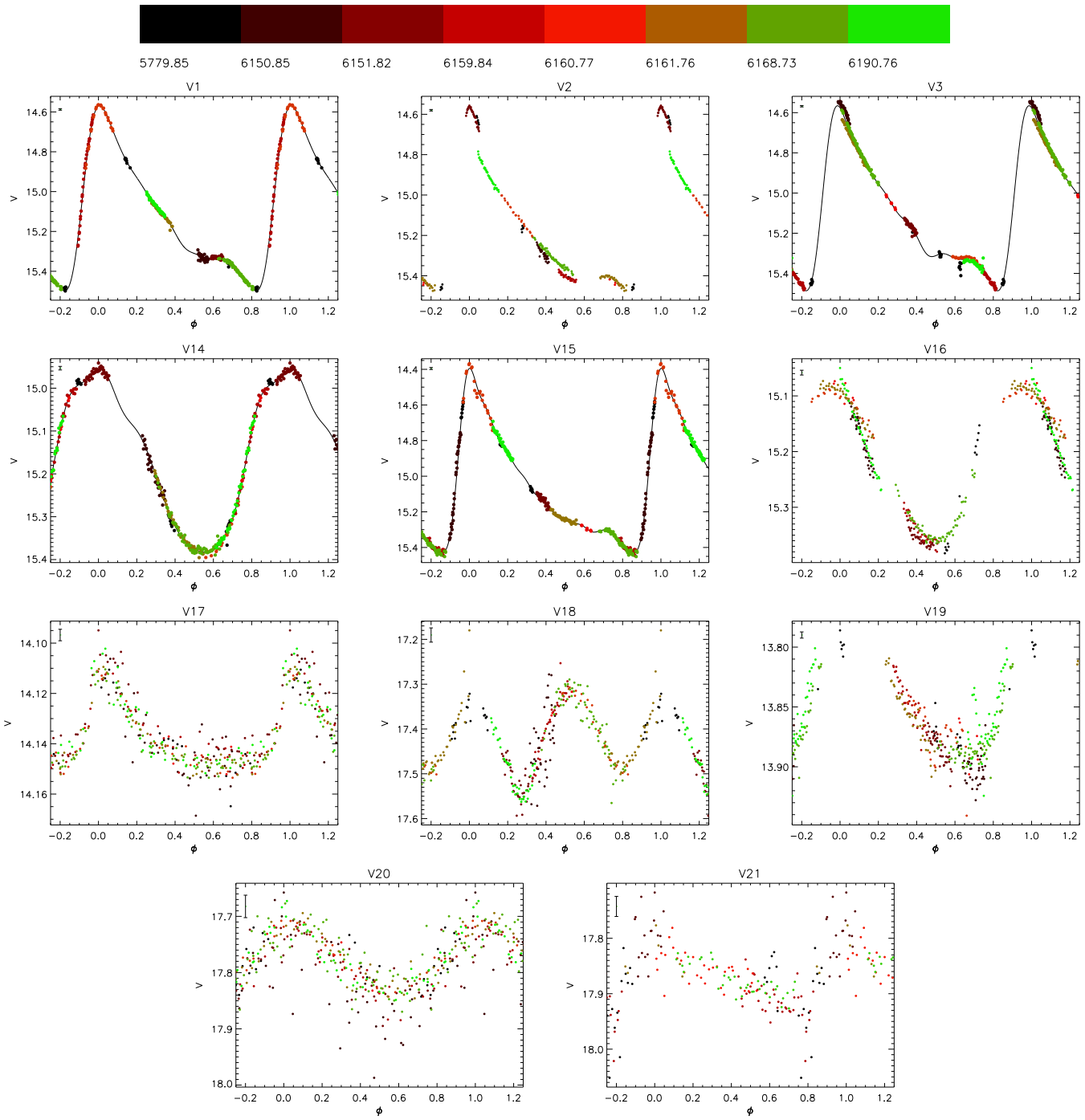

Figure 4. Phased V-band light curves of the variables with a period estimate. Different colours are used for different nights, with the colour coding given in the form of a colour bar spanning the whole time range of the observations (top panel). Fourier decomposition fits are overplotted for the objects for which those were successful.

mental period around $P_0 \sim 0.435$. We pre-whiten our data for the first-overtone period to check whether we can recover this period. In the V data, we find no evidence for such a period or any other pulsation period in our resulting power spectrum. We find similar results using the I data, leading us to conclude that the unsatisfactory phasing of the V16 light curves is not due to double-mode pulsation.

Secondly, we also tried to fit the light curve by including a secular period change. To do this, we minimise the string length, but with a time-dependent period $P(t)$ and phase $\phi(t)$,

$$P(t) = P_0 + \beta(t - E) \quad (2)$$
$$\phi(t) = (t - E)/P(t) - \lfloor (t - E)/P(t) \rfloor , \quad (3)$$

where β is the rate of change of the period and P_0 is the period at epoch E. We varied P_0 within a small range near the value we found using the string-length method, and for

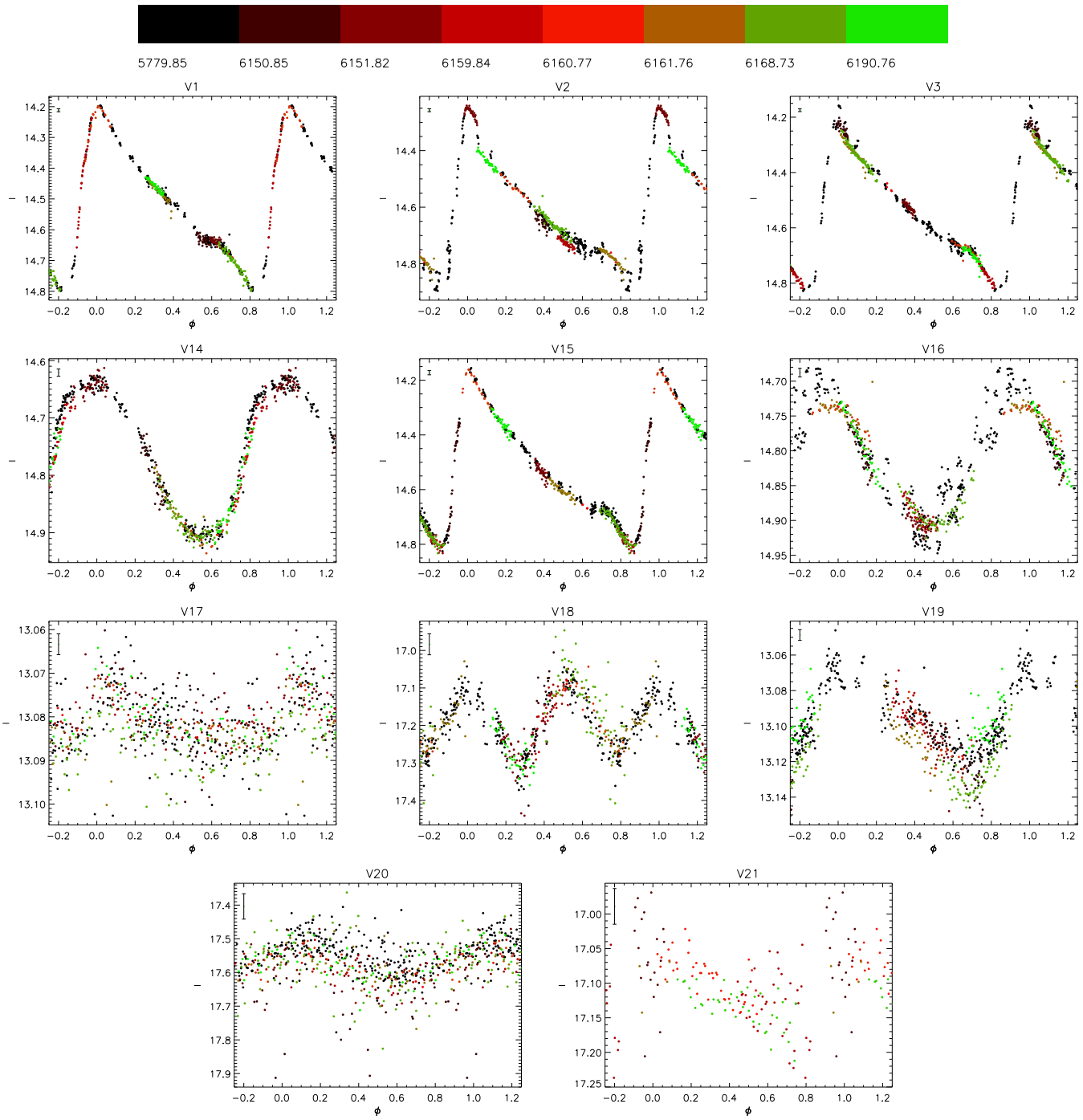

Figure 5. Same as Fig. 4 but for the I band. For V21, we only plot data points with error $\sigma < 0.3$ mag and do not plot 2011 data due to poor photometry.

each value of P_0 we explored a grid of values for β ranging between -10^{-7} and $10^{-7} dd^{-1}$. From this we found that no such secular period change can explain the scatter in our phased light curve of V16.

This leads us to conclude that V16 either exhibits the Blazhko effect, or shows signs of non-radial pulsation. Amplitude variations are clear when comparing the 2011 (black filled circles on Fig. 4 and 5) and 2012 data, and Blazhko-like effects cause period modulations as well, which would explain that the light curve is not phased properly when using a single best-fit period. On the other hand, the scatter in the light curves, particularly in the $I-$band, is very similar to that observed in light curves of some of the variables in M 55 detected by Olech et al. (1999). They concluded that the scatter in the variations were caused by non-radial oscillations, and we suggest here that non-radial pulsation could also be the source of the scatter in the light curves of V16.

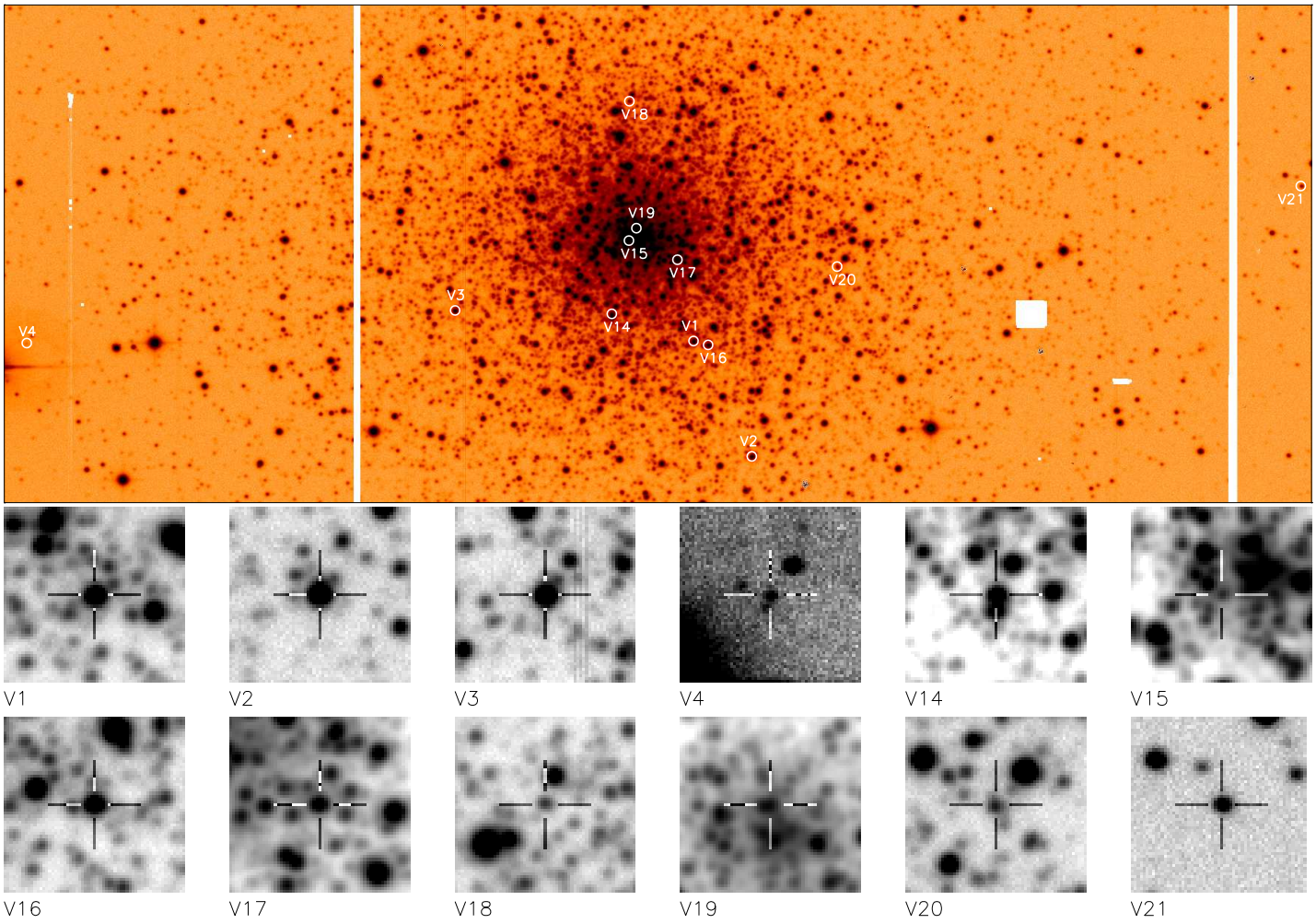

Figure 6. Finding chart for the confirmed variable objects in M 30, using our V reference image. North is up and East is to the right. The image size is 11.57 × 4.55 arcmin^2, while each stamp size is 23.4 × 23.4 arcsec^2. White circles and labels indicate the locations of the variables, and each of the variables we detect in our data is shown with a crosshair at the centre of an individual stamp. Note that the display scale of each stamp is different in order to make the source visible.

4. Fourier decomposition of RR Lyrae star light curves

Applying Fourier decomposition to the $V-$band light curves of RR Lyrae variables with sufficient phase coverage allows us to derive several of their properties, which we then use as a proxy for the parameters of their host cluster. Fourier decomposition consists in fitting light curves with the Fourier series

$$m(t) = A_0 + \sum_{k=1}^{N} A_k \cos\left[\frac{2\pi k}{P}(t-E) + \phi_k\right], \qquad (4)$$

where $m(t)$ is the magnitude at time t, N is the number of harmonics used in the fit, P is the period of the variable, E is the epoch, and A_k and ϕ_k are the amplitude and phase of the k^{th} harmonic. The Fourier parameters, which are epoch-independent, are then defined as

$$R_{ij} = A_i/A_j \qquad (5)$$
$$\phi_{ij} = j\phi_i - i\phi_j\,. \qquad (6)$$

In order to avoid over-fitting light curve features, we used the minimum number of harmonics that provided a good fit. Furthermore, for each variable, we checked the dependence on N of the parameters we derive in the next sections. We found very little variation with N, with any changes smaller than the error bars associated with the relevant quantities. In the following analysis, we excluded V16 because we suspect from its light curve that it may be affected by Blazhko effects or by non-radial pulsation (see Sec. 3.4).

We list the coefficients A_k we obtained for the first four harmonics in Table 6, as well as the Fourier parameters ϕ_{21}, ϕ_{31} and ϕ_{41} for the variables for which we could obtain a Fourier decomposition. We also list the deviation parameter D_m, defined by Jurcsik & Kovács (1996) in order to assess whether fit parameters are reliable to derive properties of the RR Lyrae variables. Although Jurcsik & Kovács (1996) used a criterion whereby fits should have $D_m < 3$ for their empirical relations to yield reliable estimates of stellar properties, a less stringent criterion of $D_m < 5$ has been used by other authors (e.g. Cacciari et al. 2005). Here

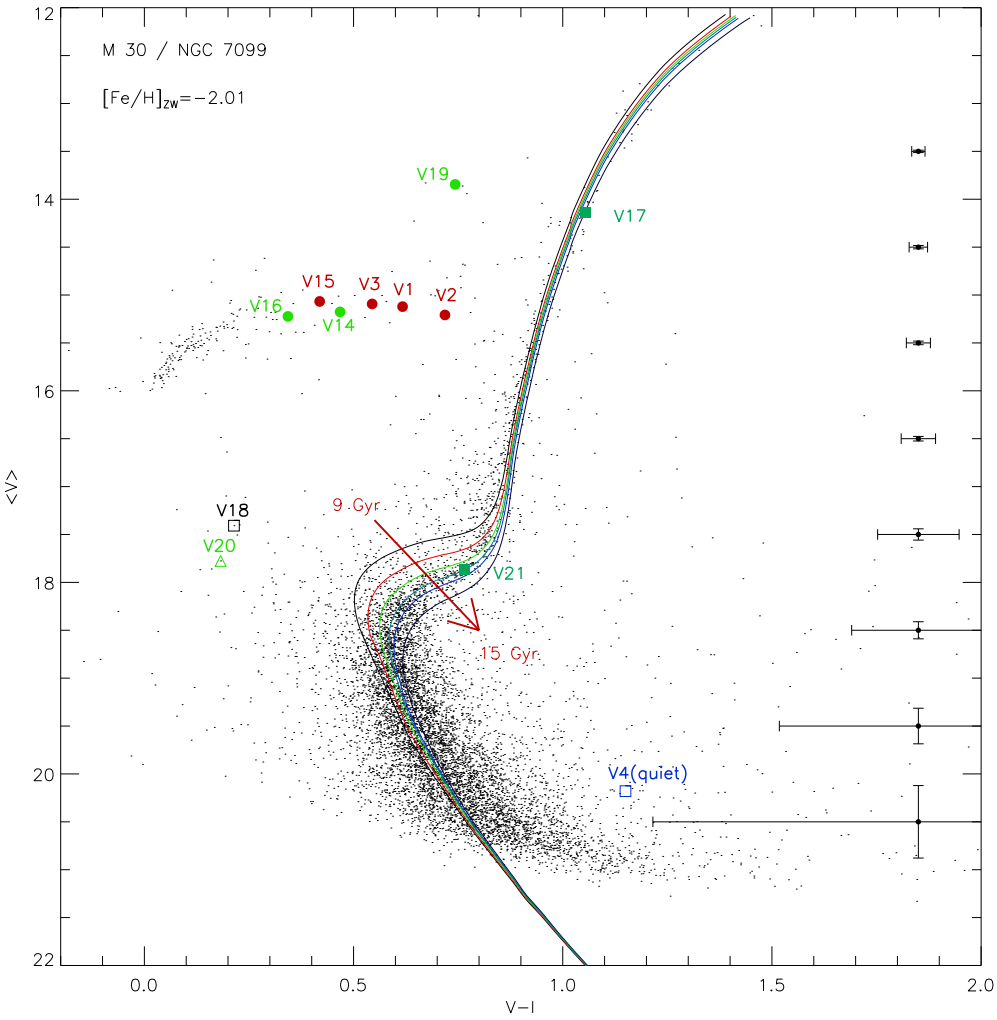

Figure 7. $(V-I), V$ colour-magnitude diagram from our photometry. The location of RR Lyrae (filled circles, RR0 in red, RR1 in green), SX Phoenicis (green triangles), U Geminorum (Blue square), eclipsing blue straggler (black open square) and other variables of uncertain type (green filled squares) are shown. On the right of the plot, typical error bars are plotted for different magnitude levels. Also plotted are isochrones from VandenBerg & Clem (2003) for ages of 9, 10.5, 12, 13.0 (our best-fit isochrone), 13.5 and 15 Gyr.

we also adopt $D_m < 5$ as a selection criterion to estimate stellar properties.

Although some acceptable fits could be obtained for V2, with $D_m < 5$, we exclude it from the analysis as well because we suspect its light curve might be affected by Blazhko effects. Furthermore, the value of the physical parameters is very sensitive to the number of harmonics used in the fit. Although we suggested in Sec. 3.4 that V3 might also be affected by Blazhko effects, we find that the Fourier fits and resulting physical parameters are stable for V3, and therefore include it in the following analysis. We note, however, that this may account for the larger value of D_m we find for V3. We also exclude V19 because our phase coverage does not enable us to find a good Fourier fit. This leaves us with 4 RR Lyrae stars with good Fourier decompositions, three RR0 (V1, V3 and V15) and one RR1 (V14).

4.1. Metallicity

We use the empirical relations of Jurcsik & Kovács (1996) to derive the metallicity [Fe/H] for each of the variables for which we could obtain a successful Fourier decomposition. The relation is derived from the spectroscopic metallicity measurement of field RR0 variables, and it relates [Fe/H] to the period P and the Fourier parameter ϕ^s_{31}, where s denotes a parameter obtained by fitting a *sine* series rather than the cosine series we fit with Eq. (4). [Fe/H] is then expressed as

$$[\mathrm{Fe/H}]_\mathrm{J} = -5.038 - 5.394\,P + 1.345\,\phi^s_{31} \qquad (7)$$

where the subscript J denotes a non-calibrated metallicity, the period P is in days, and ϕ^s_{ij} can be calculated via

$$\phi^s_{ij} = \phi_{ij} - (i-j)\,\frac{\pi}{2}\,. \qquad (8)$$

We transform these to the metallicity scale of Zinn & West (1984) (hereafter ZW) using the relation from Jurcsik (1995):

#	A_0	A_1	A_2	A_3	A_4	ϕ_{21}	ϕ_{31}	ϕ_{41}	N	D_m
RR0										
V1	15.121(2)	0.337(2)	0.160(2)	0.110(2)	0.050(2)	4.045(12)	8.498(16)	6.581(22)	7	2.6
V2[a]	15.196(2)	0.320(2)	0.134(2)	0.107(2)	0.081(2)	4.005(11)	8.511(15)	6.668(16)	7	3.0
V3	15.118(2)	0.319(2)	0.152(2)	0.112(2)	0.059(2)	3.973(11)	8.413(13)	6.468(19)	7	4.9
V15	15.067(2)	0.344(2)	0.181(2)	0.122(1)	0.081(2)	3.987(7)	8.274(12)	6.431(14)	10	2.5
RR1										
V14	15.176(2)	0.214(3)	0.030(3)	0.012(2)	0.010(2)	4.773(26)	2.673(137)	2.338(104)	6	–

Table 6. Parameters from the Fourier decomposition. A good decomposition could not be obtained for V19, due to poor phase coverage; the Fourier fit to V2 was also poor, and V16 is excluded because it shows signs of amplitude and period modulation due to Blazhko effects or non-radial pulsation. Numbers in parentheses are the 1-σ uncertainties on the last decimal place. [a]We provide our best-fit Fourier parameters but do not use the decomposition of V2 in the derivation of the cluster parameters, due to the sensitivity of the V2 parameters to the number of harmonics used.

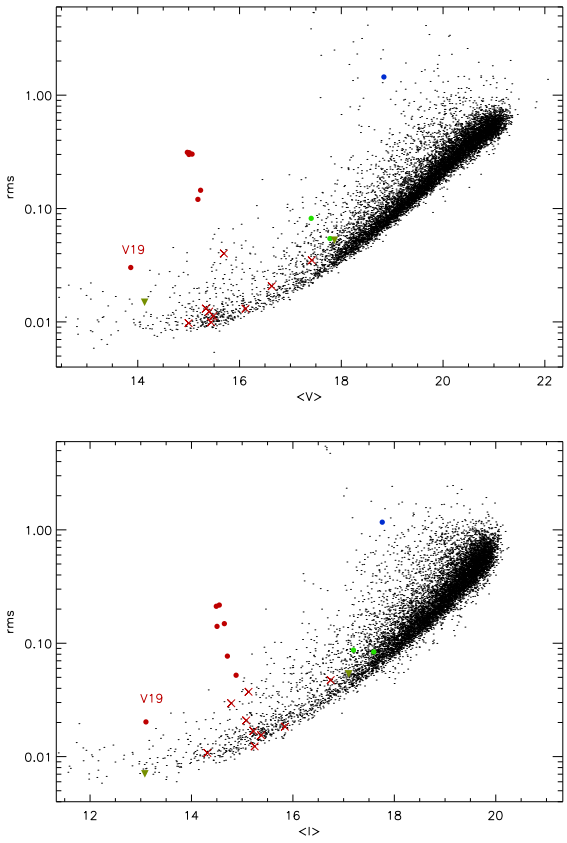

Figure 2. Plot of root mean square magnitude deviation versus mean magnitude for all stars for which photometry was obtained. Plots are for the $V-$band (top) and $I-$band (bottom). Classified variables are marked as filled circles, with RR Lyrae in red, SX Phoenicis and blue stragglers in light green, U Geminorum in blue, and variables of unknown type as dark green triangles. Non-variable objects previously catalogued as variable in the literature are marked with red crosses.

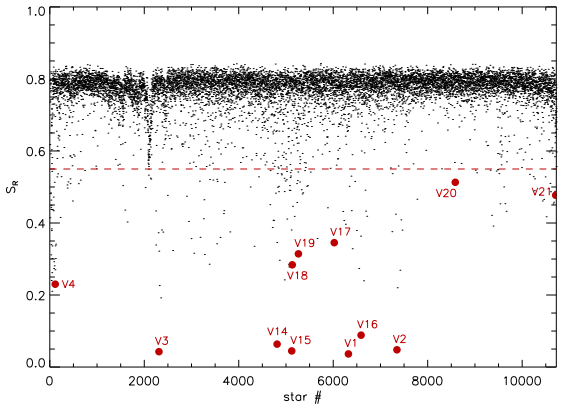

Figure 3. Plot of the distribution of the S_R statistic as defined in the text, for our V-band light curves.

#	[Fe/H]$_{\rm ZW}$	M_V	$\log(L/L_\odot)$	$T_{\rm eff}$
RR0				
V1	-2.04(2)	0.351(2)	1.780(1)	6187(7)
V3	-1.95(2)	0.428(2)	1.746(1)	6247(6)
V15	-2.01(2)	0.428(2)	1.746(1)	6249(5)
RR1				
V14	-2.03(4)	0.540(6)	1.650(3)	7180(13)

Table 7. Physical parameters for the RR Lyrae variables calculated using the Fourier decomposition parameters and the relations given in the text. Numbers in parentheses are the 1-σ uncertainties on the last decimal place.

$$[\mathrm{Fe/H}]_{\rm ZW} = \frac{[\mathrm{Fe/H}]_{\rm J} - 0.88}{1.431}. \quad (9)$$

However Kovács (2002) noted that for metal-poor clusters, Eq. (7) yields metallicity values that are too large by ~ 0.2 dex. This was also confirmed by Gratton et al. (2004) and Di Fabrizio et al. (2005) by comparing spectroscopic and Fourier-decomposition metallicity values for RR Lyrae in the Large Magellanic Cloud (LMC). Therefore here we include a shift of -0.20 dex (on the [Fe/H]$_{\rm J}$ scale) to metallicity values we derive for RR0 stars using Eq. (7), which corresponds to a shift on the ZW scale of -0.14 dex.

For the RR1 variables, we calculated the metallicity using the empirical relation of Morgan et al. (2007), linking [Fe/H], P and ϕ_{31}:

$$\begin{aligned}[\mathrm{Fe/H}]_{\rm ZW} &= 2.424 - 30.075\,P + 52.466\,P^2 \\ &\quad +0.982\,\phi_{31} + 0.131\phi_{31}^2 - 4.198\,\phi_{31}P \end{aligned} \quad (10)$$

Metallicity values calculated using Eq. (7) & (9) and (10) are given in Table 7.

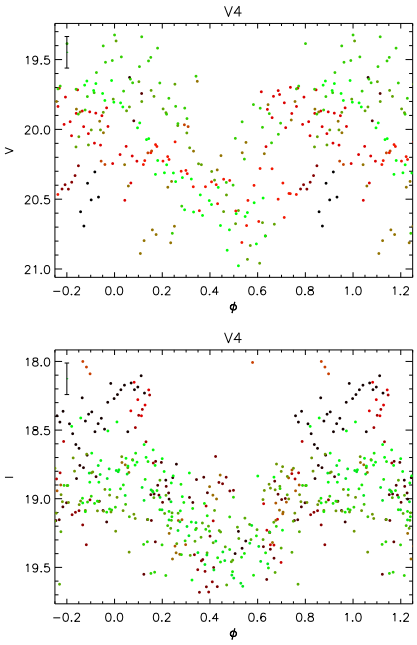

Figure 8. Phased quiescent light curves of V4 in the $V-$ (top) and I-band (bottom). Colour coding is the same as for Fig. 4. For clarity we only plot data points with errors $\sigma < 0.3$ mag.

4.2. Effective Temperature

The Fourier parameters can also be used to calculate the effective temperature, using empirical relations derived by Jurcsik (1998). Those relations link the $(V-K)_0$ colour to P as well as several of the Fourier coefficients and parameters:

$$(V-K)_0 = 1.585 + 1.257\,P - 0.273\,A_1 - 0.234\,\phi_{31}^s + 0.062\,\phi_{41}^s \quad (11)$$

$$\log T_{\rm eff} = 3.9291 - 0.1112\,(V-K)_0 - 0.0032\,[{\rm Fe/H}]_{\rm J}\,. \quad (12)$$

For RR1 variables, Simon & Clement (1993) used theoretical models to derive an empirical relation,

$$\log\,T_{\rm eff} = 3.7746 - 0.1452 \log\,P + 0.0056\,\phi_{31}\,. \quad (13)$$

We list the temperatures we derived for each RR Lyrae star in Table 7. As noted in our previous analyses, there are several caveats to deriving temperatures with Eq. (12) and (13). These relations yield values of $T_{\rm eff}$ for RR0 and RR1 stars on different absolute scales. Furthermore, the effective temperatures we derive here show systematic deviations from the relations predicted by evolutionary models of Castelli (1999) or the temperature scales of Sekiguchi & Fukugita (2000). Bearing these caveats in mind, we use these relations to derive temperature estimates in order to be consistent with our previous studies.

4.3. Absolute Magnitude

Kovács & Walker (2001) derived empirical relations to calculate V-band absolute magnitudes for the RR0 variables, linking the magnitude to Fourier coefficients through

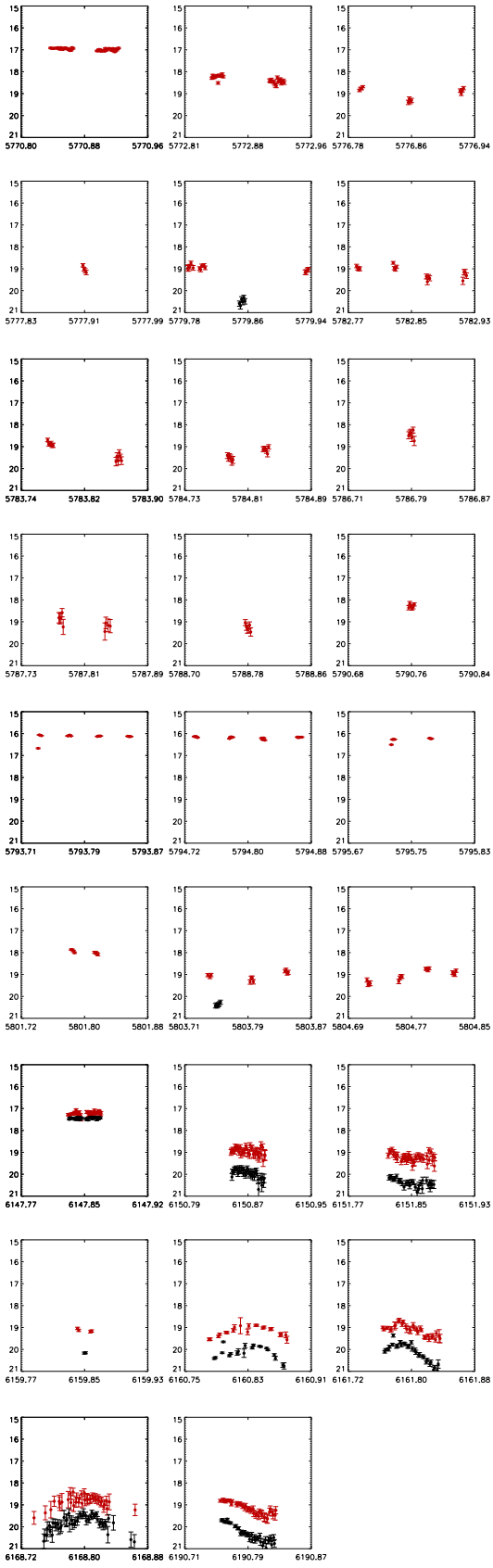

Figure 9. 2012 $V-$ and $I-$band light curves of V4. V data is plotted in black, and I data in red. For clarity we plot only data points with errors $\sigma < 0.3$ mag. The $x-$axes are given in HJD-2450000.

$$M_V = -1.876 \log P - 1.158\, A_1 + 0.821\, A_3 + K_0\,, \quad (14)$$

where K_0 is a constant. As in our previous studies, we adopt a value of $K_0 = 0.41$ mag to be consistent with a true LMC distance modulus of $\mu_0 = 18.5$ mag (Freedman et al. 2001). For RR1 variables, we use the relation of Kovács (1998),

$$M_V = -0.961\, P - 0.044\, \phi_{21}^s - 4.447\, A_4 + K_1\,, \quad (15)$$

where K_1 is a constant, for which we choose a value of 1.061 with the same justification as for our choice of K_0.

We also converted the magnitudes we obtained to luminosities using

$$\log\left(L/L_\odot\right) = -0.4\,\left[M_V + B_C(T_{\rm eff}) - M_{\rm bol,\odot}\right]\,, \quad (16)$$

where $M_{\rm bol,\odot}$ is the bolometric magnitude of the Sun, $M_{\rm bol,\odot} = 4.75$, and $B_C(T_{\rm eff})$ is a bolometric correction which we determine by interpolating from the values of Montegriffo et al. (1998) for metal-poor stars, and using the value of $T_{\rm eff}$ we derived in the previous section. Values of M_V and $\log(L/L_\odot)$ for the RR0 and RR1 variables are listed in Table 7. Using our average values of M_V, in conjunction with the average values of $[{\rm Fe/H}]_{\rm ZW}$ (Sec. 4.1), we find a good agreement with the $M_V - [{\rm Fe/H}]_{\rm ZW}$ relation derived in the literature (e.g. Kains et al. 2012, see Fig.9 of that paper).

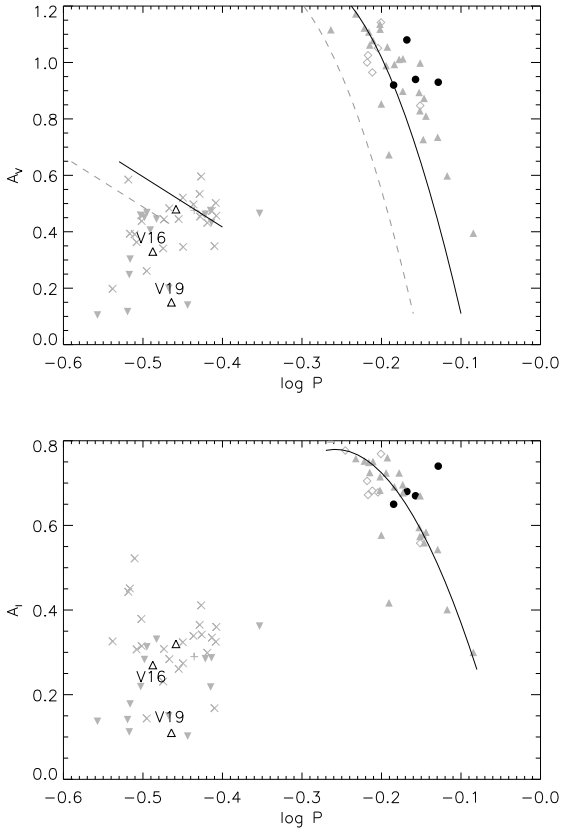

Figure 10. Bailey diagram of the light curve amplitude versus the logarithm of the period for RR Lyrae stars in M 30, in V (top) and I (bottom). RR0 variables are plotted as filled circles, and RR1 variables as open triangles; we mark the locations of V16 which we suggest is affected by Blazhko effects or non-radial pulsation, and of V19, which has an underestimated amplitude due to blending. Also plotted on the $V-$band diagram as solid lines are the relations of Cacciari et al. (2005) for evolved stars, obtained by applying a shift of +0.06 to log P in the relations derived for the Oosterhoff type I cluster M3; the original relations (without the shift of 0.06 in log P) are also plotted in light gray dashed lines. For the $I-$band we plot the relation derived by Arellano Ferro et al. (2011) for RR0 stars. For comparison we also plot the populations of RR Lyrae detected in the Oosterhoff type II clusters M 9 (Arellano Ferro et al. 2013) and NGC 5024 (Arellano Ferro et al. 2011) in light gray, with filled triangles and inverted triangles for RR0 and RR1 stars respectively. For stars with Blazhko effects, we use open diamonds for RR0 stars and crosses for RR1 stars; the star marked with a + sign is a double-mode RR1 star.

5. Cluster properties

5.1. Oosterhoff Type

We find mean periods $< P_{\rm RR0} >= 0.693 \pm 0.038$ d and $< P_{\rm RR1} >= 0.346 \pm 0.003$ d, with a proportion of 43% of the RR Lyrae in this cluster being of RR1 type.

From these values of $< P_{\rm RR0} >$ and the fraction of RR1 stars in M 30, as well as its low metallicity, we confirm previous classification of this cluster in the literature as Oosterhoff type II (e.g. Lee & Carney 1999). This is also confirmed by comparing the locations of our variables on a Bailey diagram (Fig. 10) to the tracks derived by Cacciari et al. (2005) for evolved stars.

5.2. Distance

5.2.1. Using the RR Lyrae stars

We can use the A_0 parameter from our Fourier decompositions, which corresponds to the mean apparent V magnitude of the RR Lyrae, as well as the absolute magnitudes of the RR Lyrae we derived in Sec. 4.3 to derive the distance modulus to M 30. The mean value of the A_0 for our RR0 variables is 15.09 ± 0.03 mag, while the mean of the absolute magnitudes is 0.40 ± 0.04 mag. This yields a distance modulus of $\mu = 14.69 \pm 0.05$ mag. Using the parameters for our RR1 variable (V14, see Tables 6 & 7), we find $\mu = 14.64$ mag.

The reddening towards this cluster has been estimated in the literature by several authors, with values of $E(B-V)$ ranging from 0.01 to 0.12 mag. Zinn (1980) derived a value of $E(B-V) = 0.01$ mag from integrated light measurements, Bolte (1987) adopted a value of $E(B-V) = 0.02$ mag, while Richer et al. (1988) found a value of $E(B-V) = 0.068 \pm 0.035$ mag; Piotto et al. (1990) derived $E(B-V) = 0.05$ mag from their CMD analysis, and Samus et al. (1995) found values of $E(B-V) = 0.09$ or 0.12 mag, depending on the metallicity of the isochrone they fitted to their CMD. Ferraro et al. (1999) report a value for this cluster $E(B-V) = 0.03$ mag.

Here we adopt a value of $E(B-V) = 0.03 \pm 0.01$ mag, as well as a value of $R_V = 3.1$ for our Galaxy. We use these to derive mean true distance moduli of $\mu_0 = 14.60 \pm 0.05$

mag and $\mu_0 = 14.54$ mag, from our RR0 and RR1 variables respectively. These values correspond to mean physical distances of 8.32 ± 0.20 kpc and 8.10 kpc. Since the distance values are sensitive to our chosen value of $E(B-V)$, we also derive distances using the largest value of reddening in the literature $E(B-V) = 0.12$ mag, to find a lower limit for the distances of 7.32 ± 0.17 and 7.13 kpc. Our values for the distance to the cluster are consistent with previous estimates in the literature, reported in Table 8.

5.2.2. Using SX Phoenicis stars

SX Phoenicis stars can be used as standard candles thanks to their period-luminosity ($P-L$) relation (e.g. Jeon et al. 2003), allowing us to estimate the distance to M 30 using the detected SX Phoenicis star in our sample, V20. We use the $P-L$ relation of Cohen & Sarajedini (2012),

$$M_V = -(1.640 \pm 0.110) - (3.389 \pm 0.090) \log P_f \,, \quad (17)$$

where P_f denotes the fundamental-mode pulsation period. Using $P_f = 0.040199$ d for V20, we find $M_V = 3.09 \pm 0.11$ mag. Using a mean magnitude of $< V >= 17.79$ mag, $E(B-V) = 0.03$ mag, this yields a distance modulus of 14.61 ± 0.11 mag, which corresponds to a physical distance of 8.35 ± 0.42 kpc, in excellent agreement with the distance calculated using the RR Lyrae stars, and consistent with estimates in the literature.

5.3. Metallicity

Although the relation of Sandage (2006) relating the mean period of RR0 stars to the cluster metallicity is not applicable for Oosterhoff type II clusters (Clement et al. 2001), we can use the metallicities we calculated in Sec. 4.1 for the RR Lyrae stars in the cluster to derive an estimate for the metallicity of M 30. To do this, we simply compute an average of the RR Lyrae metallicities given in Table 7, excluding the variables for which the metallicity estimate is unreliable. Assuming that there is no systematic offset between the different types of variables, as in previous studies (Kains et al. 2012; Bramich et al. 2011), we find a mean metallicity $[\mathrm{Fe/H}]_{\mathrm{ZW}} = -2.01 \pm 0.04$, in good agreement with values found in the literature (see Table 9).

Carretta et al. (2009a) derived a new metallicity scale based on GIRAFFE and UVES spectra of red giant branch (RGB) stars in 19 globular clusters, which is now widely used to quote metallicity values for globular clusters. The transformation from the ZW to the UVES (Carretta et al. 2009a) scale is given as

$$[\mathrm{Fe/H}]_{\mathrm{UVES}} = -0.413 + 0.130\,[\mathrm{Fe/H}]_{\mathrm{ZW}} - 0.356\,[\mathrm{Fe/H}]^2_{\mathrm{ZW}} \,. \quad (18)$$

Using this we find a metallicity for M 30 of $[\mathrm{Fe/H}]_{\mathrm{UVES}} = -2.11 \pm 0.06$, significantly higher than the value found for this cluster by Carretta et al. (2009b) of $[\mathrm{Fe/H}]_{\mathrm{UVES}} = -2.34 \pm 0.05$.

5.4. Age

We use our CMD to derive an estimate for the age of M 30, by fitting to it the isochrones of VandenBerg & Clem (2003), using our estimate of the cluster metallicity, $[\mathrm{Fe/H}]_{\mathrm{ZW}} = -2.01 \pm 0.04$. We also used a value for the $\alpha-$enhancement of $[\alpha/\mathrm{Fe}] = +0.2$ (Dotter et al. 2010). From the best-fitting isochrones, we estimate the age of the cluster to be 13.0 ± 1.0 Gyr, in good agreement with recent estimates in the literature (see Table 10). A set of isochrones is overplotted on the CMD in Fig. 7.

6. Conclusions

We have used $V-$ and $I-$band observations spanning a baseline of ~ 14 months to survey stellar photometric variability in M 30. This allows us to update the catalogue of variables in this cluster significantly, with detections and refined analysis of three previously known RR Lyrae stars, one known U Gem star, as well as of two candidate RR Lyrae stars, to which we assigned catalogue numbers. Furthermore, we detect previously unknown variables, including two RR1 stars, an SX Phoenicis star, an eclipsing blue straggler system, and two variables that we are unable to classify with certainty. We provide refined period estimates for all variables, and then carry out Fourier decomposition of RR Lyrae stars. Using the Fourier parameters of stars for which this was successful, we derive properties for the RR Lyrae, and use these as proxies for the cluster's properties.

We find a cluster metallicity of $[\mathrm{Fe/H}]_{\mathrm{ZW}} = -2.01 \pm 0.04$, or $[\mathrm{Fe/H}]_{\mathrm{UVES}} = -2.11 \pm 0.06$, and distances of 8.32 ± 0.20 or 8.10 kpc, using RR0 and RR1 stars respectively. Our light curve of the SX Phoenicis variable V20 also affords another way to estimate the cluster distance; using this, we find a distance of 8.35 ± 0.42 kpc. Our CMD also allows us to estimate the age of the cluster by fitting isochrones to it. We find an age of 13 ± 1 Gyr. All of these values are in good agreement with estimates in the literature, and are independent estimates calculated for the first time using Fourier decomposition of RR Lyrae in this cluster.

Acknowledgements

We thank the referee Christine Clement for constructive comments. NK acknowledges an ESO Fellowship. The research leading to these results has received funding from the European Community's Seventh Framework Programme (/FP7/2007-2013/) under grant agreement No 229517. AAF acknowledges the support of DGAPA-UNAM through project IN104612. AAF and SG are thankful to the CONACyT (México) and the Department of Science and Technology (India) for financial support under the Indo-Mexican collaborative project DST/INT/MEXICO/RP001/2008. OW (aspirant FRS - FNRS), AE (post-doc PRODEX), YD (post-doc PRODEX) and J. Surdej acknowledge support from the Communauté française de Belgique – Actions de recherche concertées – Académie universitaire Wallonie-Europe. TCH gratefully acknowledges financial support from the Korea Research Council for Fundamental Science and Technology (KRCF) through the Young Research Scientist Fellowship Program. TCH acknowledges financial support from KASI (Korea Astronomy and Space Science Institute) grant number 2012-1-410-02. KA, DB, MD, MH, and CL are supported by NPRP grant NPRP-09-476-1-78 from the Qatar National Research Fund (a member of Qatar Foundation).

Reference	μ_0 [mag]	Distance [kpc]	Method
This work	14.60 ± 0.05	8.32 ± 0.20	Fourier decomposition of RR0 light curves
This work	14.54	8.10	Fourier decomposition of RR1 light curves
This work	14.61 ± 0.11	8.35 ± 0.42	SX Phoenicis $P-L$ relation
Carretta et al. (2000)	14.88 ± 0.05	9.46 ± 0.22	Parallax of local subdwarfs
Ferraro et al. (1999)	14.71	8.75	Magnitude of the horizontal branch
Sandquist et al. (1999)	14.65 ± 0.12	8.51 ± 0.47	Parallax of local subdwarfs
Sandquist et al. (1999)	14.87 ± 0.12	9.42 ± 0.52	Parallax of local subdwarfs
Gratton et al. (1997)	14.94 ± 0.08	9.72 ± 0.36	Parallax of local subdwarfs
Bergbusch (1996)	14.83	9.25	CMD analysis
Samus et al. (1995)	14.70 ± 0.10	8.71 ± 0.40	CMD analysis
Piotto et al. (1990)	14.65 ± 0.15	8.51 ± 0.59	CMD analysis
Piotto et al. (1987)	14.50 ± 0.50	7.94 ± 1.83	CMD analysis
Bolte (1987)	14.65	8.51	Parallax of local subdwarfs

Table 8. Modulus and distance estimates for M 30 in the literature.

Reference	$[Fe/H]_{ZW}$	$[Fe/H]_{UVES}$	Method
This work	-2.01 ± 0.04	-2.11 ± 0.06	Fourier decomposition of RR Lyrae light curves
Carretta et al. (2009b)	-2.04 ± 0.16	-2.34 ± 0.05	UVES spectroscopy of red giants
Carretta et al. (2009c)	-2.05 ± 0.16	-2.36 ± 0.05	FLAMES/GIRAFFE specta of red giants
Sandquist et al. (1999)	-2.01 ± 0.09	-2.11 ± 0.14	Simultaneous reddening-metallicity method
Bergbusch (1996)	-2.03	-2.14	CMD isochrone fitting
Minniti et al. (1993)	-2.11 ± 0.08	-2.27 ± 0.13	Spectroscopy of red giants
Claria et al. (1988)	-2.4	-2.78 ± 0.20	Spectroscopy of red giants
Bolte (1987)	-2.03 ± 0.13	-2.14 ± 0.20	CMD isochrone fitting
Smith (1984)	-2.02 ± 0.14	-2.13 ± 0.22	Q'_{39} spectral index
Zinn & West (1984)	-2.13 ± 0.13	-2.31 ± 0.21	Q_{39} spectral index
Zinn (1980)	-1.96 ± 0.12	-2.04 ± 0.18	Q_{39} spectral index

Table 9. Different metallicity estimates for M 30 in the literature. Values were converted using Eq. (18) where necessary.

Reference	Age [Gyr]	Method
This work	13 ± 1	CMD isochrone fitting
Dotter et al. (2010)	13.25 ± 1.00	CMD isochrone fitting
Carretta et al. (2000)	12.3	Parallax of local subdwarfs
Bergbusch (1996)	14	CMD isochrone fitting
Samus et al. (1995)	17	CMD isochrone fitting
Samus et al. (1995)	15	CMD isochrone fitting
Piotto et al. (1990)	16 ± 2	CMD isochrone fitting
Bolte (1987)	17	CMD isochrone fitting

Table 10. Age estimates for M 30 in the literature.

The Danish 1.54m telescope is operated based on a grant from the Danish Natural Science Foundation (FNU). Funding for the Stellar Astrophysics Centre at Aarhus University is provided by The Danish National Research Foundation. This research was supported in part by the ASTERISK project (ASTERoseismic Investigations with SONG and Kepler), funded by the European Research Council (Grant agreement no.: 267864). CS received funding from the European Union Seventh Framework Programme (FP7/2007-2013) under grant agreement no. 268421. CHG and XSF acknowledge support from National Natural Science Foundation of China (grants Nos. 10373023 and 10773027). HK acknowledges support from a Marie-Curie Intra-European Fellowship.

References

Allen, C., Moreno, E., & Pichardo, B. 2006, ApJ, 652, 1150
Arellano Ferro, A., Bramich, D. M., Figuera Jaimes, R., et al. 2013, in prep.
Arellano Ferro, A., Figuera Jaimes, R., Giridhar, S., et al. 2011, MNRAS, 416, 2265
Bailey, S. I. 1902, Annals of Harvard College Observatory, 38, 1
Bergbusch, P. A. 1996, AJ, 112, 1061
Blažko, S. 1907, Astronomische Nachrichten, 175, 325
Bolte, M. 1987, ApJ, 319, 760
Bramich, D. M. 2008, MNRAS, 386, L77
Bramich, D. M., Figuera Jaimes, R., Giridhar, S., & Arellano Ferro, A. 2011, MNRAS, 413, 1275
Bramich, D. M. & Freudling, W. 2012, MNRAS, 424, 1584
Bramich, D. M., Horne, K., Albrow, M. D., et al. 2013, MNRAS, 428, 2275
Cacciari, C., Corwin, T. M., & Carney, B. W. 2005, AJ, 129, 267
Carretta, E., Bragaglia, A., Gratton, R., D'Orazi, V., & Lucatello, S. 2009a, A&A, 508, 695
Carretta, E., Bragaglia, A., Gratton, R., & Lucatello, S. 2009b, A&A, 505, 139
Carretta, E., Bragaglia, A., Gratton, R. G., et al. 2009c, A&A, 505, 117
Carretta, E., Gratton, R. G., Clementini, G., & Fusi Pecci, F. 2000, ApJ, 533, 215
Castelli, F. 1999, A&A, 346, 564
Claria, J. J., Minniti, D., & Gomez, M. N. 1988, A&A, 199, L1
Clement, C. M., Ferance, S., & Simon, N. R. 1993, ApJ, 412, 183
Clement, C. M., Muzzin, A., Dufton, Q., et al. 2001, AJ, 122, 2587

Clementini, G., Corwin, T. M., Carney, B. W., & Sumerel, A. N. 2004, AJ, 127, 938
Cohen, R. E. & Sarajedini, A. 2012, MNRAS, 419, 342
Cox, A. N., Hodson, S. W., & Clancy, S. P. 1983, ApJ, 266, 94
Darragh, A. N. & Murphy, B. W. 2012, Journal of the Southeastern Association for Research in Astronomy, 6, 72
Di Fabrizio, L., Clementini, G., Maio, M., et al. 2005, A&A, 430, 603
Djorgovski, S. & King, I. R. 1986, ApJ, 305, L61
Dotter, A., Sarajedini, A., Anderson, J., et al. 2010, ApJ, 708, 698
Echevarria, J. & Jones, D. H. P. 1984, MNRAS, 206, 919
Ferraro, F. R., Messineo, M., Fusi Pecci, F., et al. 1999, AJ, 118, 1738
Forbes, D. A. & Bridges, T. 2010, MNRAS, 404, 1203
Freedman, W. L., Madore, B. F., Gibson, B. K., et al. 2001, ApJ, 553, 47
Gratton, R. G., Bragaglia, A., Clementini, G., et al. 2004, A&A, 421, 937
Gratton, R. G., Fusi Pecci, F., Carretta, E., et al. 1997, ApJ, 491, 749
Jeon, Y.-B., Lee, M. G., Kim, S.-L., & Lee, H. 2003, AJ, 125, 3165
Jurcsik, J. 1995, Act. Astron., 45, 653
Jurcsik, J. 1998, A&A, 333, 571
Jurcsik, J. & Kovács, G. 1996, A&A, 312, 111
Kai, L. & Sheng-Bang, Q. 2012, AJ, 144, 161
Kains, N., Bramich, D. M., Figuera Jaimes, R., et al. 2012, A&A, 548, A92
Kovács, G. 1998, Mem. Soc. Astron. Ital., 69, 49
Kovács, G. 2002, in Astronomical Society of the Pacific Conference Series, Vol. 265, Omega Centauri, A Unique Window into Astrophysics, ed. F. van Leeuwen, J. D. Hughes, & G. Piotto, 163
Kovács, G. & Walker, A. R. 2001, A&A, 371, 579
Lafler, J. & Kinman, T. D. 1965, ApJS, 11, 216
Lee, J.-W. & Carney, B. W. 1999, AJ, 118, 1373
Machin, G., Callanan, P. J., Allington-Smith, J., Charles, P. A., & Hassall, B. J. M. 1991, MNRAS, 250, 602
Margon, B. & Downes, R. A. 1983, ApJ, 274, L31
Minniti, D., Geisler, D., Peterson, R. C., & Claria, J. J. 1993, ApJ, 413, 548
Monet, D. G., Levine, S. E., Canzian, B., et al. 2003, AJ, 125, 984
Montegriffo, P., Ferraro, F. R., Origlia, L., & Fusi Pecci, F. 1998, MNRAS, 297, 872
Morgan, S. M., Wahl, J. N., & Wieckhorst, R. M. 2007, MNRAS, 374, 1421
Nemec, J. M. 1985, AJ, 90, 240
Olech, A., Kaluzny, J., Thompson, I. B., et al. 1999, AJ, 118, 442
Padmanabhan, N., Schlegel, D. J., Finkbeiner, D. P., et al. 2008, ApJ, 674, 1217
Pietrukowicz, P. & Kaluzny, J. 2004, Act. Astron., 54, 19
Pietrukowicz, P., Kaluzny, J., Schwarzenberg-Czerny, A., et al. 2008, MNRAS, 388, 1111
Piotto, G., Capaccioli, M., Ortolani, S., et al. 1987, AJ, 94, 360
Piotto, G., King, I. R., Capaccioli, M., Ortolani, S., & Djorgovski, S. 1990, ApJ, 350, 662
Richer, H. B., Fahlman, G. G., & Vandenberg, D. A. 1988, ApJ, 329, 187
Rosino, L. 1949, Mem. Soc. Astron. Ital., 20, 63
Rosino, L. 1961, Asiago-Padova Cont., 117
Samus, N. N., Ipatov, A. P., Smirnov, O. M., et al. 1995, Astronomy Letters, 21, 810
Sandage, A. 2006, AJ, 131, 1750
Sandquist, E. L., Bolte, M., Langer, G. E., Hesser, J. E., & Mendes de Oliveira, C. 1999, ApJ, 518, 262
Sekiguchi, M. & Fukugita, M. 2000, AJ, 120, 1072
Simon, N. R. & Clement, C. M. 1993, ApJ, 410, 526
Skottfelt, J., Bramich, D. M., Figuera Jaimes, R., et al. 2013, ArXiv e-prints
Smith, H. A. 1984, ApJ, 281, 148
Smitka, M. T. & Layden, A. C. 2010, in Bulletin of the American Astronomical Society, Vol. 36, American Astronomical Society Meeting Abstracts 215, 606.18
Stellingwerf, R. F. 1978, ApJ, 224, 953
Stetson, P. B. 2000, PASP, 112, 925
Terzan, A. 1968, Publications of the Observatoire Haute-Provence, 9, 24
Terzan, A. & Rutily, B. 1975, A&A, 38, 307
VandenBerg, D. A. & Clem, J. L. 2003, AJ, 126, 778
Zinn, R. 1980, ApJS, 42, 19
Zinn, R. & West, M. J. 1984, ApJS, 55, 45

[1] European Southern Observatory, Karl-Schwarzschild Straße 2, 85748 Garching bei München, Germany
e-mail: nkains@eso.org
[2] Instituto de Astronomía, Universidad Nacional Autónoma de Mexico
[3] SUPA School of Physics & Astronomy, University of St Andrews, North Haugh, St Andrews, KY16 9SS, United Kingdom
[4] Niels Bohr Institute, University of Copenhagen, Juliane Maries vej 30, 2100 Copenhagen, Denmark
[5] Centre for Star and Planet Formation, Geological Museum, Øster Voldgade 5, 1350 Copenhagen, Denmark
[6] Indian Institute of Astrophysics, Koramangala 560034, Bangalore, India
[7] Qatar Foundation, P.O. Box 5825, Doha, Qatar
[8] Department of Astronomy, Boston University, 725 Commonwealth Ave, Boston, MA 02215, United States of America
[9] Dipartimento di Fisica "E.R Caianiello", Universit di Salerno, Via Ponte Don Melillo, 84084 Fisciano, Italy
[10] Istituto Nazionale di Fisica Nucleare, Sezione di Napoli, Italy
[11] HE Space Operations GmbH, Flughafenallee 24, 28199 Bremen, Germany
[12] Istituto Internazionale per gli Alti Studi Scientifici (IIASS), Vietri Sul Mare (SA), Italy
[13] Institut d'Astrophysique et de Géophysique, Université de Liège, Allée du 6 Août 17, Sart Tilman, Bât. B5c, 4000 Liège, Belgium
[14] Astronomisches Rechen-Institut, Zentrum für Astronomie der Universität Heidelberg (ZAH), Mönchhofstr. 12-14, 69120 Heidelberg, Germany
[15] Hamburger Sternwarte, Universität Hamburg, Gojenbergsweg 112, 21029 Hamburg
[16] Main Astronomical Observatory, Academy of Sciences of Ukraine, vul. Akademika Zabolotnoho 27, 03680 Kyiv, Ukraine
[17] National Astronomical Observatories/Yunnan Observatory, Chinese Academy of Sciences, Kunming 650011, China
[18] Key Laboratory for the Structure and Evolution of Celestial Objects, Chinese Academy of Sciences, Kunming 650011, China
[19] Korea Astronomy and Space Science Institute, Daejeon 305-348, Korea
[20] Institut for Rumforskning og -teknologi, Danmarks Tekniske Universitet, København, Denmark
[21] Stellar Astrophysics Centre, Department of Physics and Astronomy, Aarhus University, Ny Munkegade 120, DK-

8000 Aarhus C, Denmark

[22] Jodrell Bank Centre for Astrophysics, University of Manchester, Oxford Road,Manchester, M13 9PL, UK

[23] Max Planck Institute for Astronomy, Königstuhl 17, 69117 Heidelberg, Germany

[24] Perth Observatory, Walnut Road, Bickley, Perth 6076, Australia

[25] Department of Astronomy, Ohio State University, 140 West 18th Avenue, Columbus, OH 43210, United States of America

[26] Departamento de Astronomía y Astrofísica, Pontificia Universidad Católica de Chile, Av. Vicuña Mackenna 4860, 7820436 Macul, Santiago, Chile

[27] Department of Physics, Sharif University of Technology, P. O. Box 11155–9161, Tehran, Iran

[28] Perimeter Institute for Theoretical Physics, 31 Caroline St. N., Waterloo ON, N2L 2Y5, Canada

[29] Instituto de Astronomía - UNAM, Km 103 Carretera Tijuana Ensenada, 422860, Ensenada (Baja Cfa), Mexico

[30] Space Telescope Science Institute, 3700 San Martin Drive, Baltimore, MD 21218, United States of America

[31] INFN, Gruppo Collegato di Salerno, Sezione di Napoli, Italy

[32] Max Planck Institute for Solar System Research, Max-Planck-Str. 2, 37191 Katlenburg-Lindau, Germany

[33] Astrophysics Group, Keele University, Staffordshire, ST5 5BG, United Kingdom